

1 Atmospheric $p\text{CO}_2$ Sensitivity to the Solubility
2 Pump: The Role of the Low-Latitude Ocean

T. DeVries

3 Department of Earth System Science, University of California at Irvine,
4 Irvine, California, USA

F. Primeau

5 Department of Earth System Science, University of California at Irvine,
6 Irvine, California, USA

T. DeVries, Department of Earth System Science, University of California at Irvine, Rowland Hall, Irvine, CA 92697, USA. (tdevries@uci.edu)

F. Primeau, Department of Earth System Science, University of California at Irvine, Rowland Hall, Irvine, CA 92697, USA. (fprimeau@uci.edu)

Abstract. Previous research has shown that the atmospheric $p\text{CO}_2$ sensitivity to changes in low-latitude sea-surface chemistry (“low-latitude sensitivity”) depends on both the volume of the ocean ventilated from low latitudes and on the degree of air-sea disequilibrium at high latitudes. However, it is not clear which effect is more important. In this paper we present a diagnostic framework for quantifying the relative importance of low-latitude ventilation vs. high-latitude air-sea disequilibrium in determining the low-latitude sensitivity of ocean carbon cycle models. The diagnostic uses a Green function that partitions the ocean’s carbon inventory based on whether the carbon last interacted with the atmosphere in the low latitudes or in the high latitudes. The diagnostic is applied to a simple three-box model, a box model with a ventilated thermocline, and a suite of OGCM runs meant to capture a range of possible ocean circulations for present and last-glacial-maximum conditions. The diagnostic shows unambiguously that the OGCM has a greater low-latitude sensitivity than the box models because of the greater amount of water ventilated from low latitudes in the OGCM. However, when applied to the suite of OGCM runs, the diagnostic also reveals that the effect of high-latitude air-sea disequilibrium can sometimes dominate the effect of low-latitude ventilation, and is highly sensitive to the state of the ocean circulation. In particular, the magnitude of the high-latitude disequilibrium effect correlates strongly with the strength of the Atlantic meridional overturning circulation and the volume of water ventilated from northern high latitudes.

1. Introduction

Ice core records show that during the glacial periods of the past 800,000 years, the partial pressure of atmospheric CO₂ ($p\text{CO}_2^{\text{atm}}$) was 80-100 μatm lower than during the corresponding interglacial periods [Petit et al., 1999; Siegenthaler et al., 2005; Lüthi et al., 2008]. By increasing its store of carbon during glacial periods and decreasing it during interglacials, the ocean is believed to have played a dominant role in regulating these $p\text{CO}_2^{\text{atm}}$ variations (see reviews by Sigman and Boyle [2000] and Archer et al. [2000a]). Variations in the ocean's carbon inventory are believed to be due to changes in the operation of the ocean's carbon pump [Volk and Hoffert, 1985]. The carbon pump is that suite of processes, both physical and biological, that enrich deep ocean waters in dissolved inorganic carbon (DIC) relative to surface waters. With a fixed amount of carbon in the ocean-atmosphere system, and assuming a constant ocean alkalinity, a stronger carbon pump translates to a decrease in the inventory of carbon in the surface ocean and also in the atmosphere which equilibrates with the surface ocean.

Despite decades of research, the exact mechanism whereby the ocean regulates $p\text{CO}_2^{\text{atm}}$ on glacial-interglacial timescales remains uncertain (see, e.g., LeGrand and Alverson [2001]). One reason for this uncertainty is due to the fact that numerical models disagree on the degree to which changes in the chemistry of the low-latitude surface ocean can alter $p\text{CO}_2^{\text{atm}}$. Early box model studies [Knox and McElroy, 1984; Sarmiento and Toggweiler, 1984; Siegenthaler and Wenk, 1984] found that the relatively small area of the cold high-latitude ocean controlled the CO₂ content of the surface low-latitude ocean and of the atmosphere. Later studies pointed out that while $p\text{CO}_2^{\text{atm}}$ in simple box models

50 is relatively insensitive to changes in low-latitude sea-surface chemistry, three-dimensional
51 dynamical ocean general circulation models (OGCMs) predict a much stronger sensitivity
52 [*Bacastow, 1996; Broecker et al., 1999*]. Low-latitude sensitivity is important because of
53 the large surface area of the low-latitude as compared to the high-latitude oceans. As
54 pointed out by *Bacastow [1996]* a strong low-latitude sensitivity implies that changes
55 in the low-latitude sea-surface temperature could contribute significantly to the glacial-
56 interglacial $p\text{CO}_2^{atm}$ changes.

57 Various mechanisms have been proposed to explain the discrepancy between the low-
58 latitude sensitivity of box models and OGCMs. *Archer et al. [2000b]* suggested that
59 diffusive mixing in OGCMs enhanced their low-latitude sensitivity, and showed that a
60 2-dimensional circulation model could be made to span the range of sensitivities of box
61 models and OGCMs by adjusting the diffusive mixing in the model, with higher diffusiv-
62 ities producing higher low-latitude sensitivities. *Follows et al. [2002]* showed that simple
63 box models were missing important circulation features, resulting in weak low-latitude
64 sensitivities. By adding a box representing the ventilated thermocline to a 3-box model,
65 *Follows et al. [2002]* showed that the sensitivity of the box model could be made to match
66 that of an OGCM. On the other hand, *Toggweiler et al. [2003]* explained the same dif-
67 ferences in sensitivity as being due to differences in the degree of air-sea disequilibrium
68 at high-latitude ventilation sites. *Toggweiler et al. [2003]* showed that OGCMs support a
69 greater air-sea disequilibrium than box models, and suggested that this was the ultimate
70 reason for the higher low-latitude sensitivity of OGCMs as compared to box models.

71 These studies showed that there are two effects that contribute to setting low-latitude
72 sensitivity. The first is the amount of water ventilated from the low latitudes. The second

73 is the degree of air-sea disequilibrium at high-latitude ventilation sites. Distinguishing
74 between the two effects is important because, as pointed out by *Toggweiler et al.* [2003],
75 the former affects nutrient cycling as well, whereas the latter does not, since nutrients
76 do not exchange with the atmosphere. In this way atmospheric $p\text{CO}_2$ sensitivity to the
77 solubility pump can be de-coupled from sensitivity to the biological pump. Clearly, a
78 method for quantifying the relative importance of air-sea disequilibrium and the size of
79 the water mass ventilated from low latitudes would help us better understand the role of
80 the low-latitude oceans in regulating atmospheric $p\text{CO}_2$ on glacial-interglacial timescales.
81 In this article we develop a diagnostic formula that allows us to separate and quantify
82 the effects of low-latitude ventilation and high-latitude air-sea disequilibrium on the total
83 low-latitude sensitivity of ocean carbon cycle models.

84 The key new development which helps us to address the issue of low-latitude sensitivity
85 is the introduction of a Green function which diagnoses the fraction of the ocean volume
86 ventilated from any given patch on the ocean surface. We use the Green function to show
87 that the sensitivity of $p\text{CO}_2^{atm}$ to low-latitude solubility perturbations can be expressed
88 as the sum of three terms: (1) a term that is dependent on the volume of the ocean
89 ventilated from low latitudes and independent of air-sea disequilibrium, (2) a term that
90 is dependent on both the volume of the ocean ventilated from high latitudes and the
91 air-sea disequilibrium in high latitudes, and (3) a term that is dependent on the volume
92 of the ocean ventilated from low latitudes and the air-sea disequilibrium in low latitudes.
93 The magnitudes of these three effects can be diagnosed from a perturbation experiment
94 without the need to rerun the model with fast air-sea gas exchange.

95 The goals of this study are to quantify the magnitudes of the low-latitude ventilation
96 and high-latitude air-sea disequilibrium effects in different types of models, to explore the
97 sensitivity of each effect to the ocean circulation, and to clarify the mechanisms influenc-
98 ing their magnitudes. To make contact with previous work on the issue of low-latitude
99 sensitivity, we revisit the question of why OGCMs are more low-latitude sensitive than
100 box models. We compare the low-latitude sensitivities of the 3-box model of *Toggweiler*
101 *et al.* [2003], the 5-box model with an explicit thermocline box of *Follows et al.* [2002],
102 and a 3-dimensional abiotic carbon cycling model based on the OGCM of *Primeau* [2005].
103 Our diagnostic clearly shows that the difference between the low-latitude sensitivities of
104 the three models is due to differences in the amount of water ventilated from the low
105 latitudes.

106 We also compare the low-latitude sensitivity of several different versions of the OGCM
107 with different surface boundary conditions and different eddy diffusivity parameters. We
108 find that low-latitude sensitivities in this suite of OGCM runs vary by more than a factor of
109 2, and depend critically on the state of the ocean circulation. Our diagnostic reveals that
110 most of the variability in low-latitude sensitivity is due to variability in the effect of high-
111 latitude air-sea disequilibrium. The disequilibrium effect is strengthened by increasing
112 the strength of the meridional overturning circulation, and by the partitioning of more
113 deep-water ventilation to the North Atlantic. Variability in low-latitude sensitivity is also
114 caused by variability in the amount of water ventilated from low latitudes, which generally
115 increases with higher wind stresses and higher diffusivities, and in the buffering capacity
116 of the ocean, which increases with higher mean ocean temperature and with lower mean
117 ocean $p\text{CO}_2$.

2. Theory

2.1. Factors influencing low-latitude sensitivity

118 To illustrate how the sensitivity of $p\text{CO}_2^{atm}$ is related to the redistribution of carbon in
119 the ocean-atmosphere system, Figure 1 shows the sense of the carbon flow between the
120 atmospheric, surface- and deep-ocean reservoirs as the system adjusts to a cooling per-
121 turbation at the surface of the low-latitude ocean. (Following *Bacastow* [1996]; *Broecker*
122 *et al.* [1999]; *Follows et al.* [2002] we use the example of a low-latitude cooling perturbation
123 without taking into account its effect on the ocean circulation to illustrate the sensitivity
124 of the solubility pump to low-latitude perturbations.) A decrease in ocean temperature
125 increases the solubility of CO_2 , causing a net flow of carbon from the atmosphere into the
126 low-latitude surface ocean. Subduction and mixing processes transport the surface-ocean
127 carbon anomaly into the interior ocean. At the same time, the decreased atmospheric
128 $p\text{CO}_2$ and the increased carbon in the ocean causes an anomalous out-gassing of CO_2
129 at high latitudes. This flow of carbon from the high-latitude ocean to the atmosphere
130 constitutes a negative feedback that tends to decrease the $p\text{CO}_2^{atm}$ sensitivity to a low-
131 latitude perturbation. As a result of this redistribution of carbon the system ultimately
132 settles into a new equilibrium state. How far this new equilibrium is from the one before
133 the perturbation was applied (i.e. the low-latitude sensitivity) depends on the amount of
134 water that is ventilated directly from low latitudes, and also on the air-sea gas exchange
135 rate and the surface residence time of waters in the high latitudes, which govern how
136 much of the anomalous carbon is released back to the atmosphere.

137 Both of these effects were originally discussed in a series of papers investigating the
138 reason why OGCMs are more low-latitude sensitive than box models. As suggested by

139 *Broecker et al.* [1999] and *Archer et al.* [2000b], and clearly demonstrated by *Follows*
140 *et al.* [2002], the low-latitude sensitivity of $p\text{CO}_2^{\text{atm}}$ depends on the amount of water
141 ventilated from the low-latitude surface ocean. This ventilation can in principle occur
142 through diffusive mixing, as suggested by *Archer et al.* [2000b], but direct measurements
143 of diffusivity in the tropical pycnocline [*Ledwell et al.*, 1993] suggest that this method
144 of ventilation is quite weak. Rather, the formation of a ventilated thermocline in the
145 subtropical gyres, as demonstrated by *Follows et al.* [2002], is the dominant low-latitude
146 mode of ventilation. For the case of a low-latitude cooling, ventilation processes carry the
147 carbon rich surface anomaly into the interior ocean, sequestering carbon in the interior
148 ocean and allowing surface waters to take up more carbon from the atmosphere. On the
149 other hand, *Toggweiler et al.* [2003] highlighted the importance of air-sea disequilibrium
150 in influencing low-latitude sensitivity. High-latitude air-sea disequilibrium increases low-
151 latitude sensitivity because it tends to suppress the outgassing of anomalous carbon at
152 high latitudes, thereby retaining a larger amount of carbon in the ocean.

2.2. Separating the effects of low-latitude ventilation and air-sea disequilibrium on low-latitude sensitivity

153 In this section we derive a formula that allows us to quantify the relative impacts of air-
154 sea disequilibrium and low-latitude ventilation on the low-latitude sensitivity of a model.
155 Following *Ito and Follows* [2003] we consider the carbon mass balance for the ocean-
156 atmosphere system, but instead of separating the ocean carbon inventory into upper-
157 and deep-ocean pools we separate the ocean carbon inventory into high- and low-latitude
158 pools, where by high-latitude pool we mean the carbon that was last in contact with the
159 atmosphere at high latitudes and by low-latitude pool we mean the carbon that was last

160 in contact with the atmosphere at low latitudes. More precisely,

$$161 \quad C_{total} = M_a p\text{CO}_2^{atm} + \text{DIC}_L + \text{DIC}_H, \quad (1)$$

162 where M_a is the molar mass of the atmosphere and where DIC_L and DIC_H are respectively
 163 the low- and high-latitude dissolved inorganic carbon pools. Such a decomposition is made
 164 possible through the use of the volume integrated Green function $\mathcal{G}(\mathbf{r}_s)$ (e.g. *Primeau*
 165 [2005]).

166 $\mathcal{G}(\mathbf{r}_s)$ can be interpreted as the volume of the ocean per unit surface area, that was last in
 167 contact with the atmosphere at the point \mathbf{r}_s on the surface of the ocean. A computationally
 168 efficient procedure for computing $\mathcal{G}(\mathbf{r}_s)$ is presented in the supplemental material, but an
 169 intuitive understanding of how to compute it is all that is needed to understand our results.
 170 To compute the value of \mathcal{G} for a particular patch of the surface ocean, one can think of
 171 labeling (in a sense, “coloring”), fluid elements as they enter the patch, and removing the
 172 color label as soon as a fluid element makes surface contact outside the patch. Taking
 173 the whole-ocean inventory, at steady-state, of colored fluid elements labeled in this way,
 174 yields the volume of the ocean ventilated through that particular patch. Performing this
 175 procedure for every grid point in the model, and dividing by the area of each grid box,
 176 yields the full spatial distribution $\mathcal{G}(\mathbf{r}_s)$.

177 Because $\mathcal{G}(\mathbf{r}_s)$ has units of length, it can also be thought of as an “effective thickness”
 178 [*Primeau*, 2005], where the greatest effective thicknesses correspond to places that ven-
 179 tilate the largest part of the interior ocean. The integral of $\mathcal{G}(\mathbf{r}_s)$ over the entire ocean
 180 surface Ω gives the total ocean volume,

$$181 \quad V_{oce} = \int_{\Omega} \mathcal{G}(\mathbf{r}_s) d^2r_s$$

$$= \underbrace{\int_{\Omega_L} \mathcal{G}(\mathbf{r}_s) d^2 r_s}_{V_L} + \underbrace{\int_{\Omega_H} \mathcal{G}(\mathbf{r}_s) d^2 r_s}_{V_H}, \quad (2)$$

where in the second line we have partitioned the ocean volume into a volume V_L that was last ventilated through a low-latitude surface patch Ω_L , and a volume V_H that was last ventilated through a high-latitude surface patch Ω_H , with the union of the two regions covering the entire ocean surface. Figure 2 shows a plot of $\mathcal{G}(\mathbf{r}_s)$ for one of the OGCM circulations analyzed in this paper, as well as the regions covered by Ω_L and Ω_H .

The total ocean DIC inventory that cycles through the solubility pump is given by the convolution of $\mathcal{G}(\mathbf{r}_s)$ and the surface DIC field, i.e.

$$\begin{aligned} \text{DIC}_{oce} &= \int_{\Omega} \text{DIC}(\mathbf{r}_s) \mathcal{G}(\mathbf{r}_s) d^2 r_s, \\ &= \underbrace{\int_{\Omega_L} \text{DIC}(\mathbf{r}_s) \mathcal{G}(\mathbf{r}_s) d^2 r_s}_{\text{DIC}_L} + \underbrace{\int_{\Omega_H} \text{DIC}(\mathbf{r}_s) \mathcal{G}(\mathbf{r}_s) d^2 r_s}_{\text{DIC}_H}. \end{aligned} \quad (3)$$

To separate the effects of air-sea disequilibrium and low-latitude ventilation on the sensitivity of $p\text{CO}_2^{atm}$ to low-latitude perturbations, we relate the surface ocean DIC concentration to the atmospheric CO_2 content and a local air-sea disequilibrium function,

$$\begin{aligned} \text{DIC}(\mathbf{r}_s) &= F(p\text{CO}_2^{oce}(\mathbf{r}_s)) \\ &= F(p\text{CO}_2^{atm} - \Delta p\text{CO}_2(\mathbf{r}_s)) \end{aligned} \quad (4)$$

where $\Delta p\text{CO}_2 \equiv p\text{CO}_2^{atm} - p\text{CO}_2^{oce}$ is the air-sea disequilibrium function and F represents the equilibrium CO_2 system for seawater. Note that in the limit of infinitely fast air-sea gas exchange $\Delta p\text{CO}_2 = 0$ and $p\text{CO}_2^{atm} = p\text{CO}_2^{oce}$.

We now consider a perturbation to low-latitude temperature that causes a redistribution of carbon between the atmosphere and ocean. (We should note that while we develop our theory in the context of a temperature perturbation, our results apply equally well to

any perturbation to low-latitude sea-surface chemistry. One must simply replace the derivatives with respect to temperature with those with respect to alkalinity, salinity, or DIC.) Taking the derivative of (1) with respect to temperature we obtain

$$M_a \frac{dp\text{CO}_2^{atm}}{dT} + \frac{d\text{DIC}_L}{dT} + \frac{d\text{DIC}_H}{dT} = 0. \quad (5)$$

As already mentioned we neglect the change in the ocean circulation due to the temperature perturbation so that $d\mathcal{G}(\mathbf{r}_s)/dT = 0$. In this case, the derivative of DIC_L with respect to a low-latitude temperature perturbation can be expanded into the following expression

$$\begin{aligned} \frac{d\text{DIC}_L}{dT} &= \int_{\Omega_L} \frac{d\text{DIC}(\mathbf{r}_s)}{dT} \mathcal{G}(\mathbf{r}_s) d^2r_s, \\ &= \int_{\Omega_L} \left[\frac{\partial F}{\partial T} + \frac{\partial F}{\partial p\text{CO}_2^{oce}} \left(\frac{dp\text{CO}_2^{atm}}{dT} - \frac{d\Delta p\text{CO}_2}{dT} \right) \right] \mathcal{G} d^2r_s, \end{aligned} \quad (6)$$

where in the second line we have dropped the spatial dependencies in \mathcal{G} , $\Delta p\text{CO}_2$, and F for notational convenience, a convention we retain in the equations that follow. The expression for $d\text{DIC}_H/dT$ is similar, except that the integral is taken over Ω_H ,

$$\frac{d\text{DIC}_H}{dT} = \int_{\Omega_H} \left[\frac{\partial F}{\partial T} + \frac{\partial F}{\partial p\text{CO}_2^{oce}} \left(\frac{dp\text{CO}_2^{atm}}{dT} - \frac{d\Delta p\text{CO}_2}{dT} \right) \right] \mathcal{G} d^2r_s. \quad (7)$$

In the above expressions, the partial derivative of F with respect to T represents the change in DIC, holding $p\text{CO}_2^{oce}$ fixed, due to the temperature dependence of the solubility coefficient and of the equilibrium constants in the sea-water CO_2 system. The partial derivative of F with respect to $p\text{CO}_2^{oce}$ represents the change in DIC, holding temperature fixed, due to the change in the sea-surface partial pressure of CO_2 .

Substituting (6) and (7) into (5), solving for $dp\text{CO}_2^{atm}/dT$ and multiplying through by δT (which is 0 on Ω_H since the temperature perturbation is confined to the low latitudes)

223 yields

$$\begin{aligned}
 224 \quad M_{oa} \delta pCO_2^{atm} &= - \int_{\Omega_L} \mathcal{G} \frac{\partial F}{\partial T} \delta T d^2 r_s \\
 225 \quad &+ \int_{\Omega_H} \mathcal{G} \frac{\partial F}{\partial pCO_2^{oce}} \delta \Delta pCO_2 d^2 r_s \\
 226 \quad &+ \int_{\Omega_L} \mathcal{G} \frac{\partial F}{\partial pCO_2^{oce}} \delta \Delta pCO_2 d^2 r_s.
 \end{aligned} \tag{8}$$

227 where $M_{oa} \equiv M_a + \int_{\Omega} \mathcal{G} \frac{\partial F}{\partial pCO_2^{oce}} d^2 r_s$.

228 Eq. (8) is a diagnostic that quantifies the effects discussed in Section 2.1. The first term
 229 on the right-hand side quantifies the direct effect of low-latitude ventilation in carrying the
 230 carbon perturbation into the deep ocean. We call this the “low-latitude ventilation effect”.
 231 This is the effect that *Follows et al.* [2002] showed to be an important factor in determining
 232 the greater low-latitude sensitivity of OGCMs as compared to box models. OGCMs
 233 ventilate more of the interior ocean through the low latitudes, because of the downward
 234 Ekman pumping and the formation of a ventilated thermocline, so that $\mathcal{G}(\mathbf{r}_s)$ is bigger in
 235 low latitudes and thus for a given temperature change there is a larger perturbation in
 236 pCO_2^{atm} . The second term on the right-hand side quantifies how high-latitude ventilation
 237 interacts with the air-sea disequilibrium in high latitudes to affect pCO_2^{atm} . It captures the
 238 effect that *Toggweiler et al.* [2003] had in mind when they suggested that differences in the
 239 high-latitude air-sea disequilibrium between box models and OGCMs could explain their
 240 different low-latitude sensitivities. The greater the high-latitude air-sea disequilibrium,
 241 the more important this effect becomes. The last term on the right-hand side quantifies
 242 how low-latitude ventilation interacts with the air-sea disequilibrium in low latitudes to
 243 affect pCO_2^{atm} . This term is generally small enough to be negligible. Note that with

244 infinitely fast air-sea gas exchange both ΔpCO_2 and $d\Delta pCO_2/dT$ vanish so that the last
 245 two terms cannot contribute to low-latitude sensitivity.

246 M_{oa} measures the total inertia of the ocean-atmosphere system, and is closely tied to
 247 the buffering capacity of the ocean. M_{oa} can be related to the total “buffered carbon”
 248 inventory of the ocean-atmosphere system, defined by *Goodwin et al.* [2007, 2008] as

$$249 \quad I_B = M_a pCO_2^{atm} + V \frac{\overline{DIC}}{R_{global}}, \quad (9)$$

250 where \overline{DIC} is the globally averaged DIC concentration and R_{global} is the globally-averaged
 251 Revelle buffer factor defined [*Goodwin et al.*, 2007]

$$252 \quad R_{global} = \frac{\partial pCO_2}{\partial \overline{DIC}} \frac{\overline{DIC}}{pCO_2^{atm}}. \quad (10)$$

253 Combining (9) and (10) and using the fact that

$$254 \quad \int_{\Omega} \mathcal{G} \frac{\partial F}{\partial pCO_2} d^2 r_s \equiv V \frac{\partial \overline{DIC}}{\partial pCO_2}, \quad (11)$$

255 we obtain the relation

$$256 \quad M_{oa} = \frac{I_B}{pCO_2^{atm}}. \quad (12)$$

257 M_{oa} can also be thought of as an inverse sensitivity, where sensitivity S measures the
 258 change in atmospheric pCO_2 due to a change in the ocean carbon inventory [*Marinov*
 259 *et al.*, 2008b],

$$260 \quad S = \frac{\delta pCO_2^{atm}}{\delta DIC_{oce}} \equiv M_{oa}^{-1}. \quad (13)$$

261 The relationships (12) and (13) show that sensitivity is directly proportional to pCO_2 ,
 262 as shown by *Marinov et al.* [2008b, a], and inversely proportional to the buffered carbon
 263 inventory I_B , as shown by [*Goodwin et al.*, 2009].

264 In the following section we will introduce the models used in this study. For each model
265 we will use the diagnostic formula (8) to determine the relative contribution of low-latitude
266 ventilation and high-latitude air-sea disequilibrium to the total low-latitude sensitivity of
267 the model.

3. Models and methods

3.1. Model design

268 For the 3-box model calculations we use the so-called “Harvardton Bear” model [*Ba-*
269 *castow*, 1996; *Knox and McElroy*, 1984; *Sarmiento and Toggweiler*, 1984; *Siegenthaler*
270 *and Wenk*, 1984]. It consists of 3 ocean boxes coupled to a well-mixed atmospheric box
271 (Figure 3a). Model parameters not given in the caption to Figure 3 are the same as those
272 used in *Toggweiler et al.* [2003]. No biology is included in the model.

273 For the 5-box model calculations we used the thermocline box model of *Follows et al.*
274 [2002]. The low-latitude surface ocean is split into two boxes representing the tropical
275 and sub-tropical ocean (Figure 3b). The interior ocean is partitioned into a deep box and
276 thermocline box, with the thermocline box ventilated through the sub-tropical ocean.

277 For the OGCM calculations we use the same circulation model used in *Primeau* [2005];
278 *Primeau and Holzer* [2006]; *Kwon and Primeau* [2006, 2008] coupled to a well-mixed at-
279 mospheric box. The ocean model uses the time-averaged flow field from a coarse-resolution
280 three-dimensional dynamical ocean circulation model forced with seasonally varying cli-
281 matological winds, sea-surface temperatures, and sea-surface salinities, as described in
282 *Primeau* [2005]. The equilibrium solution to the abiotic OGCM was found using New-
283 ton’s method as described in *Kwon and Primeau* [2006].

284 We also obtained 12 new circulations with our OGCM by restoring the model to different
285 sea-surface temperature and salinity climatologies, and by using different zonal wind stress
286 forcings and different background diffusivities. Each model was spun up for 3000 years
287 and the steady-state advective-diffusive flow was extracted as described in *Primeau* [2005].
288 The different combinations of surface boundary conditions and diffusivities for each run
289 are described in Table 1.

290 To facilitate comparison among all of the models we made some minor modifications
291 to the original model formulations. First, we used the equilibrium constants for the CO₂
292 system recommended by *Zeebe and Wolf-Gladrow* [2001] in all models. Second, we did
293 not include virtual fluxes of carbon due to evaporation and precipitation. Third, we used
294 a uniform piston velocity of 5.5×10^{-5} m/s to drive air-sea gas exchange, as in *Follows*
295 *et al.* [2002]. Finally, when computing the ocean-side $p\text{CO}_2$ we used a uniform salinity of
296 34.7 psu and a uniform alkalinity of 2341 $\mu\text{mol}/\text{kg}$, following the formula in *Follows et al.*
297 [1996].

3.2. Sensitivity experiments

298 With each model we performed two runs to diagnose the low-latitude sensitivity:

299 1. A control run in which the total carbon inventory is adjusted so that $p\text{CO}_2^{\text{atm}}$ is 278
300 μatm . The same total carbon inventory was kept for run 2.

301 2. A temperature perturbation run in which we simulated a cooling of the low-latitude
302 sea surface by reducing the temperature at which the equilibrium constants of the CO₂
303 system are computed by 6 °C, as in *Bacastow* [1996]. For the 3-box model, the low-latitude
304 sea surface is the interface between box L and the atmosphere. For the 5-box model, the

305 low-latitude sea surface is the interface between boxes T and ST and the atmosphere. For
306 the OGCM, we picked the low-latitude sea-surface to be between 45°S and 45°N, in accord
307 with *Follows et al.* [2002]. In all the runs, the physical transport model was “offline” and
308 did not respond dynamically to the imposed temperature perturbation.

309 Our metric for determining the low-latitude sensitivity of each model is simply the
310 change in $p\text{CO}_2^{\text{atm}}$ induced by a change of -6 °C in the low-latitude temperature (i.e. the
311 difference in $p\text{CO}_2^{\text{atm}}$ between runs 1 and 2).

312 For the experiments in which we compared the box models and the OGCM, we also
313 ran analogues of runs 1 and 2 under conditions of “fast gas exchange”. In these runs
314 the air-sea gas exchange piston velocity was increased uniformly so that the $p\text{CO}_2$ of the
315 surface ocean was nowhere more than 1 μatm greater or less than that of the atmosphere,
316 as in *Toggweiler et al.* [2003]. The piston velocity in the box models was increased by 100
317 times, and that in the OGCM by 500 times, relative to the control run to achieve this
318 condition. The total carbon inventory was kept the same as in runs 1 and 2. The fast gas
319 exchange sensitivities provide a check to ensure that (8) correctly diagnoses the effects
320 of air-sea disequilibrium from runs 1 and 2, without having to run the fast gas exchange
321 models.

322 As already mentioned, we did not include the dynamical effects of the low-latitude
323 temperature change in our experiments. One reason for ignoring the sensitivity of the
324 ocean circulation to low-latitude temperature perturbations is to obtain consistency with
325 previous studies [*Bacastow*, 1996; *Broecker et al.*, 1999; *Follows et al.*, 2002]. Another
326 reason is that the circulation change induced by a cooling confined to low latitudes would
327 be an *ad-hoc* representation of the true ocean response to surface cooling such as occurred

328 during glacial periods, since the actual cooling is likely to have been applied unevenly
329 across the entire ocean surface, including the high latitudes. Rather than guess the right
330 temperature perturbation to apply in the high latitude regions in the OGCM, we chose
331 to run the OGCM under the different boundary conditions shown in Table 1 to simulate
332 a range of possible ocean circulation states, and then to compare the low-latitude sensi-
333 tivities of the different model runs using the procedure described above. These runs give
334 a sense of how changes in ocean circulation can affect the low-latitude sensitivity.

4. Results and Discussion

4.1. Comparison of box models and an OGCM

335 Both the amount of water ventilated from low latitudes [*Follows et al.*, 2002] and the
336 air-sea disequilibrium in high latitudes [*Toggweiler et al.*, 2003] have been implicated in
337 enhancing the low-latitude sensitivity of OGCMs as compared to box models. One of the
338 goals of this study is to present a quantitative assessment of the relative importance of
339 each mechanism. Table 2 shows the low-latitude sensitivity of the box models and our
340 standard OGCM, separated according to Eq. (8) into a low-latitude ventilation effect, a
341 high-latitude air-sea disequilibrium effect, and a low-latitude disequilibrium effect. The
342 $p\text{CO}_2^{\text{atm}}$ sensitivity of the OGCM to the low-latitude perturbation is more than twice that
343 of the 3-box model, and about 70% greater than that of the 5-box model. Our diagnostic
344 shows that the low-latitude ventilation effect is much stronger in the OGCM than in either
345 of the box models. The high-latitude disequilibrium effect is slightly higher in the OGCM
346 than in the box models, and the low-latitude disequilibrium effect is nearly negligible in
347 all of the models.

348 Our results show that the OGCM has a higher low-latitude sensitivity than the box mod-
349 els because the OGCM ventilates more water from low latitudes. This is in accord with
350 *Follows et al.* [2002] who showed that the presence of a ventilated thermocline enhances
351 low-latitude sensitivity. Nevertheless, air-sea disequilibrium is an important contributor
352 to low-latitude sensitivity in all three models. The high-latitude disequilibrium effect ac-
353 counts for most of the low-latitude sensitivity of the 3-box model, 1/2 the sensitivity of
354 the 5-box model, and more than 1/3 of the sensitivity of the standard OGCM. As we
355 will show in Section 4.2, the magnitude of the high-latitude disequilibrium effect is highly
356 sensitive to wind stress forcing, diffusivity, and the partitioning of deep-ocean ventilation
357 between northern and southern sources. In fact, the high-latitude disequilibrium effect
358 can be greater than the low-latitude ventilation effect.

359 Table 2 also shows the low-latitude sensitivity of the fast gas exchange models (numbers
360 in parentheses). In the fast gas exchange runs, the $p\text{CO}_2$ of the surface ocean is nowhere
361 more than $1 \mu\text{atm}$ different from $p\text{CO}_2^{\text{atm}}$, so that there is almost perfect air-sea equili-
362 bration. The results are as expected. The air-sea disequilibrium effects approach zero,
363 and only the low-latitude ventilation effect remains. The magnitude of the low-latitude
364 ventilation effect is nearly the same as in the standard sensitivity runs. The slightly
365 larger low-latitude sensitivity in the fast gas exchange models is due to a reduction in
366 the inertia M_{oa} which occurs because of a reduction in the buffered carbon inventory.
367 These results indicate that it is not necessary to run additional experiments with fast gas
368 exchange in order to separate the effects of low-latitude ventilation from those of air-sea
369 disequilibrium. It is sufficient to compute the three terms in Eq. (8) for the standard
370 sensitivity experiments (runs 1 and 2) in order to know the magnitudes of these effects.

371 For this reason, we will not show results of the fast gas exchange models for the remaining
372 experiments.

4.2. Comparison of OGCM runs with different circulations

373 The results from Section 4.1 show that in a realistic ocean circulation model both the
374 low-latitude ventilation effect and the high-latitude disequilibrium effect play a significant
375 role in determining the ocean's low-latitude sensitivity. It is thus worthwhile to explore
376 what mechanisms might influence the magnitudes of each of these effects in the real ocean,
377 as well as the uncertainty in the magnitudes of each effect. To this end we performed the
378 alternate OGCM runs with the boundary conditions and eddy diffusivity parameters given
379 in Table 1. Each of the runs produces a new circulation and temperature field. We have
380 also included two runs in which last glacial maximum (LGM) temperature and salinity
381 reconstructions from *Paul and Schafer-Neth* [2003] are used as boundary conditions in
382 the model. These runs are not meant to produce definitive versions of the actual ocean
383 circulation at the LGM, but are added to help constrain the uncertainty in low-latitude
384 sensitivities by expressing different circulation regimes that could have occurred during
385 the LGM. In all, the alternate OGCM runs are meant to span a reasonable range of
386 uncertainty in the state of the ocean circulation, so that we can gain a sense of how
387 low-latitude sensitivity depends on the state of the ocean circulation.

388 Table 3 shows the low-latitude sensitivity of the 13 different versions of our OGCM.
389 The drop in atmospheric $p\text{CO}_2$ following low-latitude cooling ranges from $11.30 \mu\text{atm}$
390 in run WL2, to $24.66 \mu\text{atm}$ in run LGM1. In all runs both the low-latitude ventilation
391 effect and the high-latitude disequilibrium effect contribute significantly to the total low-
392 latitude sensitivity. The low-latitude disequilibrium effect remains negligible and will be

393 ignored in our discussion. Our theory and model results will reveal two simple scaling
 394 relationships which show that low-latitude sensitivity depends most critically on three
 395 factors: the volume of low-latitude waters, the strength of the meridional overturning
 396 circulation, and the volume of northern high-latitude waters.

397 We first consider what mechanisms influence the magnitude of the low-latitude venti-
 398 lation effect. Under conditions of complete air-sea CO₂ equilibration, we can write the
 399 atmospheric pCO₂ sensitivity to a low-latitude temperature perturbation as

$$400 \quad \delta pCO_2^{atm}|_{vent} = -M_{oa}^{-1} \int_{\Omega_L} \mathcal{G} \frac{\partial F}{\partial T} \delta T d^2 r_s, \quad (14)$$

401 which is simply the first term in (8). From (14) we see that if the state of the CO₂
 402 system chemical equilibria is approximately constant across all the models (i.e. M_{oa} and
 403 dF/dT are approximately the same), then to a good approximation the magnitude of the
 404 low-latitude ventilation effect should scale directly with the volume V_L of water ventilated
 405 from low-latitudes, since

$$406 \quad \delta pCO_2^{atm}|_{vent} \propto \int_{\Omega_L} \mathcal{G} d^2 r_s \equiv V_L. \quad (15)$$

407 This is precisely the relationship intuited by *Broecker et al.* [1999] and shown clearly in
 408 the model comparison study of *Follows et al.* [2002].

409 Figure 4(a) shows that the magnitude of the low-latitude ventilation effect does scale
 410 linearly with the volume of the ocean ventilated from low latitudes. The scatter in the
 411 plot is due to variations in the inertia M_{oa} (Table 4), which depends on the buffering
 412 capacity of the ocean. Accounting for this effect by dividing V_L by M_{oa} eliminates the
 413 scatter, as shown in the inset plot in Figure 4(a). (A perfect correlation is guaranteed by
 414 (14) as long as $\partial F/\partial T$ is the same in all runs.) Since the initial atmospheric pCO₂ was

415 kept at $278 \mu\text{atm}$ for all runs, (12) shows that variations in M_{oa} are due to variations in
 416 the buffered carbon inventory. The buffered carbon inventory is sensitive to the ocean
 417 circulation through the influence of the ocean circulation on the mean ocean chemistry.
 418 In general the buffered carbon inventory increases with higher mean ocean temperature
 419 and with lower mean ocean CO_2 concentration.

420 Our results show that the magnitude of the low-latitude ventilation effect is relatively
 421 constant across a wide range of ocean circulations. Figure 4(a) shows that increasing the
 422 background vertical diffusivity or the surface wind stress (red symbols) from the standard
 423 cases (S1 and S2) both increase the volume of low-latitude water and enhance low-latitude
 424 sensitivity, while decreasing either of these two factors (blue symbols) reduces low-latitude
 425 sensitivity. On the other hand, reducing vertical diffusivity in a high wind-stress regime
 426 increases the volume of low-latitude waters (run WHKL). However, the differences are
 427 relatively small in all cases. From these results it appears that the magnitude of the low-
 428 latitude ventilation effect is well constrained, and that the solubility effects of low-latitude
 429 cooling cannot explain a significant portion of the glacial-interglacial $p\text{CO}_2^{\text{atm}}$ variability
 430 without taking into account the effect of high-latitude air-sea disequilibrium.

431 The high-latitude air-sea disequilibrium effect is generally smaller than the low-latitude
 432 ventilation effect in our runs, but there is more variability across our suite of runs implying
 433 a greater uncertainty about its importance in explaining glacial-interglacial $p\text{CO}_2^{\text{atm}}$
 434 variability. Ignoring the low-latitude ventilation and disequilibrium terms, we can write
 435 the atmospheric $p\text{CO}_2$ sensitivity to a low-latitude temperature perturbation as

$$436 \quad \delta p\text{CO}_2^{\text{atm}}|_{\text{diseq}} = M_{oa}^{-1} \int_{\Omega_H} \mathcal{G} \frac{\partial F}{\partial p\text{CO}_2^{\text{oce}}} \delta \Delta p\text{CO}_2 d^2 r_s, \quad (16)$$

437 which is just the second term on the right-hand side of (8). Assuming that the state
 438 of the CO₂ system equilibria is approximately constant across all runs (i.e. M_{oa} and
 439 $\partial F/\partial pCO_2$ are constant), then differences in the high-latitude disequilibrium effect across
 440 the runs should scale with the volume of water ventilated from the high latitudes and the
 441 disequilibrium anomaly in high latitudes produced by the low-latitude cooling,

$$442 \quad \delta pCO_2^{atm}|_{diseq} \propto \int_{\Omega_H} \mathcal{G} \delta \Delta pCO_2 d^2 r_s. \quad (17)$$

443 To rid (17) of the convolution integral, we make the simplifying assumption that the dise-
 444 quilibrium anomaly is uniform at both the northern and southern high-latitude ventilation
 445 sites. Under these conditions, (17) reduces to

$$446 \quad \delta pCO_2^{atm}|_{diseq} \propto V_S \delta \Delta pCO_{2_S} + V_N \delta \Delta pCO_{2_N} \quad (18)$$

447 where V_S and V_N are the volumes of water ventilated from the southern and northern
 448 high latitudes, respectively.

449 Equation (18) shows that the magnitude of the high-latitude disequilibrium effect is
 450 influenced by the magnitude of the disequilibrium anomalies in the southern and northern
 451 high latitudes, as well as the partitioning of deep ocean ventilation between southern and
 452 northern sources. Our results show that disequilibrium driven through the northern high
 453 latitudes is generally larger than that driven through the Southern Ocean, and is also
 454 more sensitive to the state of the ocean circulation. For this reason we will focus on
 455 mechanisms influencing the disequilibrium anomaly in the northern high latitudes.

456 In the Atlantic Ocean, the meridional overturning circulation (AMOC) transports low-
 457 latitude water northward where it is transformed into NADW (Figure 1). It is intuitively
 458 clear that speeding up the AMOC enhances air-sea disequilibrium in the high latitudes

459 by reducing the surface residence time of poleward-flowing water parcels. Slowing down
 460 the AMOC has the opposite effect. Although the exact relationship between the strength
 461 of the AMOC and the air-sea disequilibrium in high latitudes is complicated by diffusive
 462 mixing, we show in the Appendix that for purely advective flow and relatively small
 463 perturbations to the MOC strength, δpCO_2 scales linearly with the strength of the
 464 AMOC. The linear relationship holds as long as the surface residence time is long compared
 465 to the air-sea equilibration timescale (see equation A10). If these conditions are met, then
 466 we can use (18) to write

$$467 \quad \delta pCO_2^{atm}|_{diseq}^N \propto V_N \text{AMOC} \quad (19)$$

468 where we have focussed only on the component of disequilibrium driven through the
 469 northern high latitudes, as indicated by the N superscript.

470 Figure 4(b) shows that the relationship (19) holds remarkably well in our OGCM. In the
 471 main plot we have shown only that portion of the high-latitude disequilibrium effect that
 472 is due to ventilation from areas north of 45°N (obtained by evaluating the integral (16) on
 473 Ω_H north of 45°N). The disequilibrium effect is highly sensitive to the state of the ocean
 474 circulation through the dependence of the AMOC strength and the volume of northern-
 475 source waters on wind stress and vertical diffusivity. Table 4 shows that increasing wind
 476 stress in our model both strengthens the AMOC and partitions more ventilation to the
 477 north Atlantic, which increases the magnitude of the northern high-latitude disequilibrium
 478 effect according to the simple theory (19). Changing the vertical diffusivity κ_v produces
 479 two competing effects. On one hand, increasing κ_v increases the strength of the AMOC
 480 (Table 4), which tends to increase $\delta pCO_2^{atm}|_{diseq}^N$. This scaling of MOC strength with
 481 diffusivity in coarse-resolution OGCMs is a well-known effect [*Bryan, 1987; Gnanadesikan,*

1999]. On the other hand, reducing κ_v partitions more of the deep-ocean ventilation to the north Atlantic, which also increases the northern high-latitude disequilibrium effect. In most of the runs the two effects nearly cancel, but run KL1 partitions so much more ventilation to the North Atlantic that there is a significant increase (compared to run S1) in the magnitude of the northern high-latitude disequilibrium effect, as well as the high-latitude disequilibrium effect as a whole. When both vertical diffusivity is decreased and wind stress is increased (run WHKL) the AMOC strengthens, more water is ventilated from the North Atlantic, and the high-latitude disequilibrium effect is enhanced.

The inset plot in Figure 4(b) shows the weaker and less variable disequilibrium effect that is driven through ventilation in the Southern Ocean, as a function of the fraction of the ocean ventilated south of 45°S. The Southern Ocean disequilibrium effect shows some clear trends if one focusses solely on the effects of changing one parameter. For example increasing wind stress increases the air-sea disequilibrium effect in the Southern Ocean, perhaps due to stronger Ekman pumping associated with stronger westerly winds, while weaker vertical diffusivities reduce the magnitude of the disequilibrium effect in the Southern Ocean by partitioning more ventilation to the north Atlantic. Overall though we could find no clear relationship to explain the variation across all runs. Exchange of low-latitude waters with the Southern Ocean does not follow the simple MOC pattern of the north Atlantic, and is most likely driven by mesoscale eddy transport [Gnanadesikan, 1999].

Run LGM1 is a particularly interesting case, because the high-latitude disequilibrium effect is actually larger than the low-latitude ventilation effect. This run highlights the potentially large impact of northern hemisphere air-sea disequilibrium on low-latitude

505 sensitivity. This large impact occurs because the circulation state of LGM1 produces
506 relatively rapid overturning circulation and large volumes NADW. The low-latitude ven-
507 tilation effect in run LGM1 is comparable in magnitude to the rest of the runs. This
508 emphasizes the point that the low-latitude ventilation effect and the high-latitude dise-
509 quilibrium effect are two separate effects which are not necessarily correlated.

5. Summary and conclusions

510 In this article we developed a diagnostic formula to quantitatively assess the relative
511 importance of both low-latitude ventilation and high-latitude air-sea disequilibrium in
512 setting the low-latitude sensitivity of abiotic ocean carbon cycle models. We applied
513 the formula to sensitivity experiments in which we simulated cooling of the low-latitude
514 surface ocean in two box models and a suite of OGCMs. Our goals were to quantify the
515 magnitudes of the low-latitude ventilation and high-latitude air-sea disequilibrium effects,
516 to explore the sensitivity of each effect to different ocean circulations, and to clarify the
517 mechanisms influencing the magnitude of each effect.

518 Our main theoretical result is summarized by Eq. (8), which in conjunction with our
519 experiments tells us the following:

520 1. In the limit of infinitely fast gas exchange (i.e. $\Delta pCO_2 = 0$), low-latitude sensitivity
521 depends directly on the volume V_L of the ocean ventilated from low latitudes, that is, on
522 the value of \mathcal{G} on Ω_L . As shown clearly by *Follows et al.* [2002], low-latitude sensitivity is
523 weaker in simple box models without a representation of the ventilated thermocline than
524 in OGCMs. Our diagnostic confirms that the weak low-latitude sensitivity of simple box
525 models is due to the smaller volume of low-latitude water in box models compared to

526 OGCMs, rather than to differences in high-latitude air-sea disequilibrium. A suite of ex-
527 periments with a coarse-resolution OGCM further confirms the direct correlation between
528 the amount of water V_L ventilated from low latitudes and the low-latitude sensitivity.
529 Increasing the background vertical diffusivity or the surface wind stress from their basic
530 states, increases V_L and enhances low-latitude sensitivity. Small deviations from a direct
531 correlation between V_L and low-latitude sensitivity are found to be due to variations in
532 the buffering capacity of the ocean across model runs.

533 2. For finite gas exchange, air-sea disequilibrium in the high latitudes increases low-
534 latitude sensitivity, as suggested by *Toggweiler et al.* [2003]. The magnitude of this “high-
535 latitude disequilibrium effect” depends directly on the degree of high-latitude air-sea dis-
536 equilibrium and on the volume of the ocean ventilated from high latitudes. Models in
537 which air-sea gas exchange is restricted in the high latitudes where deep waters form will
538 have large low-latitude sensitivities, as claimed by *Toggweiler et al.* [2003]. Our suite of
539 OGCM experiments shows that the magnitude of the high-latitude disequilibrium effect
540 is highly sensitive to the state of the ocean circulation and can approach or exceed that
541 of the low-latitude ventilation effect. Much of the variation in the disequilibrium effect
542 across our suite of OGCM runs can be explained by considering flow from the low latitudes
543 to the high latitudes to be purely advective. This leads to a model which predicts that
544 the magnitude of the high-latitude disequilibrium effect scales directly with the strength
545 of the meridional overturning circulation (MOC). We showed that this relationship holds
546 very well for the water masses forming in the northern high latitudes. Variations in sur-
547 face wind stress and vertical diffusivity produce highly variable low-latitude sensitivities

548 by varying the MOC strength and by modifying the partitioning of deep-ocean ventilation
549 between southern and northern sources.

550 On the whole, our results do not support a very large role for low-latitude solubility
551 perturbations in explaining glacial-interglacial $\text{pCO}_2^{\text{atm}}$ variations. Based on the exper-
552 iments presented in this paper, we believe that the part of the low-latitude sensitivity
553 which is driven by direct ventilation of the interior ocean from the low latitudes is fairly
554 well constrained, and probably not a significant source of glacial-interglacial $\text{pCO}_2^{\text{atm}}$ vari-
555 ability. However, we have identified some intriguing uncertainty in the degree to which
556 high-latitude disequilibrium can affect the low-latitude sensitivity. Under conditions of
557 rapid meridional overturning and large volumes of water ventilating from the North At-
558 lantic, low-latitude sensitivity can be significantly enhanced. The effect may be even
559 greater with extensive sea ice inhibiting gas exchange. The state of the ocean circulation
560 at the LGM remains highly uncertain [*Wunsch, 2003; Gebbie and Huybers, 2006; Huybers*
561 *et al., 2007*]. Because of this, until the LGM ocean circulation can be better constrained
562 we cannot rule out the possibility of low-latitude solubility perturbations contributing in
563 some significant way to the glacial-interglacial $\text{pCO}_2^{\text{atm}}$ variability.

564 A final point we would like to make is to caution against applying the results in this
565 paper to the biological pump. For example, it would be untrue to claim that $\text{pCO}_2^{\text{atm}}$
566 sensitivity to perturbations to low-latitude biological productivity is related to the sen-
567 sitivity to low-latitude solubility perturbations. The diagnostic presented here, and our
568 analysis, is applicable only to the solubility pump. The component critical to the biologi-
569 cal pump that we have not included in our framework is the pool of regenerated carbon in
570 the ocean. The physics governing the transport of regenerated carbon are different from

571 those governing the transport of DIC. Therefore, the response of the ocean-atmosphere
 572 system to perturbations in the biological pump could be very different from the response
 573 to perturbations in the solubility pump. Green functions analogous to the one presented
 574 in this paper can be defined for the regenerated carbon transport pathways, allowing for
 575 a framework similar to the one presented here to be developed for the biological pump.
 576 We plan to address this issue in a future paper.

Appendix A: High-latitude air-sea disequilibrium response to a low-latitude solubility perturbation

577 In this section we derive an analytic expression for the air-sea disequilibrium in high
 578 latitudes, and show how the anomalous air-sea disequilibrium in high latitudes due to
 579 a low-latitude temperature perturbation scales with the strength of the meridional over-
 580 turning circulation. The expressions are derived for a simple 3-box model without mixing,
 581 but as shown in Section 4.2 the relationships also apply well to results from the OGCM.

582 Consider the simple case where the ocean surface is divided into two regions: a low-
 583 latitude region and a high-latitude region. Advection transports water from the low-
 584 latitudes to the high latitudes, as in the 3-box model (Figure 3a). At steady-state in the
 585 high-latitude region, there exists a distribution of fluid elements with different residence
 586 times in that region. The air-sea disequilibrium is given by the mass-weighted integral of
 587 the air-sea disequilibrium of all fluid parcels, i.e.

$$588 \quad \Delta pCO_2 = \int_0^\infty Q(\tau) \Delta pCO_2(\tau) d\tau, \quad (A1)$$

589 where $\mathcal{Q}(\tau)$ is the residence-time PDF and $\Delta pCO_2(\tau)$ is the air-sea disequilibrium of
 590 water parcels with residence time τ . $\mathcal{Q}(\tau)$ has the functional form

$$591 \quad \mathcal{Q}(\tau) = \frac{1}{\tau_c} \exp(-\tau/\tau_c), \quad (\text{A2})$$

592 where $\tau_c \equiv V/M$ is a mean surface residence time defined by the volume V of the high-
 593 latitude box and the strength M of the overturning circulation.

594 The air-sea disequilibrium as a function of residence time τ can be derived from the dif-
 595 ferential equation governing the equilibration of DIC between the atmosphere and ocean,

$$596 \quad \frac{dDIC}{d\tau} = -\frac{vA\alpha}{V}(pCO_2 - pCO_2^{atm}) = \kappa\Delta pCO_2 \quad (\text{A3})$$

597 where V is the volume of the ocean in m^3 , v is the piston velocity in m/yr , A is the surface
 598 area of the ocean in m^2 , α is the solubility of CO_2 in $mol/kg/atm$, and $\kappa = vA\alpha/V$. Since
 599 DIC is a function of pCO_2 we can write

$$600 \quad \frac{dDIC}{d\tau} = \frac{\partial DIC}{\partial pCO_2} \frac{dpCO_2}{d\tau}, \quad (\text{A4})$$

601 and substitute this equation into (A3) and integrate to obtain

$$602 \quad \Delta pCO_2(\tau) = \Delta pCO_{20} \exp(-\tau/\tau_g) \quad (\text{A5})$$

603 where $\tau_g \equiv (1/\kappa)(\partial DIC/\partial pCO_2)$ is the gas exchange timescale.

604 Combining (A1), (A2), and (A5) yields,

$$605 \quad \Delta pCO_2 = \frac{\Delta pCO_{20}}{\tau_c} \int_0^\infty \exp[-\tau(1/\tau_c + 1/\tau_g)] d\tau, \quad (\text{A6})$$

606 which can be integrated to obtain an expression for the steady-state air-sea disequilibrium
 607 as a function of the initial disequilibrium and two timescales: the gas exchange timescale
 608 and the surface residence timescale,

$$609 \quad \Delta pCO_2 = \Delta pCO_{20} \frac{\tau_g}{\tau_c + \tau_g}. \quad (\text{A7})$$

610 The initial air-sea disequilibrium in the high latitudes depends on the air-sea disequi-
 611 librium in the low latitudes as well as the temperature gradient between the low- and
 612 high-latitude surface oceans, i.e.

$$613 \quad \Delta pCO_{2_0} = \Delta pCO_2^L + \frac{\partial pCO_2}{\partial T}(T^L - T^H). \quad (A8)$$

614 Assuming non-linearities in the CO₂ system equilibrium are small enough so that τ_g is
 615 the same both before and after the low-latitude temperature perturbation, the change in
 616 the high-latitude air-sea disequilibrium is given by

$$617 \quad \delta\Delta pCO_2 \approx (\delta\Delta pCO_2^L + \frac{\partial pCO_2}{\partial T}\delta T^L)\frac{\tau_g}{\tau_c + \tau_g}. \quad (A9)$$

618 In the experiments that we performed the magnitude of the temperature perturbation
 619 $\delta\Delta T$ was a constant 6°C. Additionally, the air-sea disequilibrium in the low latitudes is
 620 always small so that to a good approximation $\delta\Delta pCO_2^L$ is a constant. Thus the change
 621 in the high-latitude air-sea disequilibrium is proportional to the ratio of the gas exchange
 622 and surface residence timescales,

$$623 \quad \delta\Delta pCO_2 \simeq K\frac{\tau_g}{\tau_c + \tau_g}, \quad (A10)$$

624 where the constant K is negative for a negative temperature perturbation in the low
 625 latitudes.

626 Eq. (A10) predicts that the change in high-latitude air-sea disequilibrium after a pertur-
 627 bation to low-latitude temperature should be sensitive to the surface residence timescale,
 628 which depends on the strength of the meridional overturning circulation M . The sensitiv-
 629 ity of $\delta\Delta pCO_2$ to a change in M can be estimated by expanding (A10) in a Taylor series

630 about a reference value M_0 .

$$631 \quad \delta\Delta pCO_2 = K \left[\frac{\tau_g V \delta M}{(V + \tau_g M_0)^2} - \frac{\tau_g^2 V \delta M^2}{(V + \tau_g M_0)^3} \right] + \dots \quad (\text{A11})$$

632 The second-order term can be ignored as long as

$$633 \quad \left| \frac{\delta M}{M_0} \right| \ll \frac{\tau_{c0}}{\tau_g} + 1, \quad (\text{A12})$$

634 where τC_0 is the reference mean surface residence time corresponding to M_0 . Under
 635 these conditions $\delta\Delta pCO_2$ scales linearly with a change in the strength of the meridional
 636 overturning circulation M .

637 **Acknowledgments.** TD would like to thank the members of his PhD thesis advisory
 638 committee Ellen Druffel, Keith Moore, and John Southon. The authors would also like
 639 to thank Eun-Young Kwon for making the code for the implicit ocean biogeochemistry
 640 model available. Finally, we would like to thank the two anonymous reviewers for their
 641 constructive comments. This research was funded by the National Science Foundation
 642 grants OCE 0726871 and OCE 0623647.

References

- 643 Antonov, J. I., R. A. Locarnini, T. P. Boyer, A. V. Mishonov, and H. E. Garcia (2006),
 644 Volume 2: Salinity, in *NOAA Atlas NESDIS*, vol. 62, edited by S. Levitus, U.S. Gov-
 645 ernment Printing Office, Washington, D.C.
- 646 Archer, D., A. Winguth, D. Lea, and N. Mahowald (2000a), What caused the
 647 glacial/interglacial atmospheric pCO_2 cycles?, *Reviews of Geophysics*, 38(2), 159–189.
- 648 Archer, D. E., G. Eshel, A. Winguth, W. Broecker, R. Pierrehumbert, M. Tobis, and
 649 R. Jacob (2000b), Atmospheric pCO_2 sensitivity to the biological pump in the ocean,

- 650 *Global Biogeochemical Cycles*, 14(4), 1219–1230.
- 651 Bacastow, R. B. (1996), The effect of temperature change of the warm surface waters of
652 the oceans on atmospheric CO₂, *Global Biogeochemical Cycles*, 10(2), 319–333.
- 653 Broecker, W., J. Lynch-Stieglitz, D. Archer, M. Hoffman, E. Maier-Reimer, O. Marchal,
654 T. Stocker, and N. Gruber (1999), How strong is the Harvardton-Bear constraint?,
655 *Global Biogeochemical Cycles*, 13(4), 817–820.
- 656 Bryan, F. (1987), Parameter Sensitivity of Primitive Equation Ocean General Circulation
657 Models, *Journal of Physical Oceanography*, 17, 970–985.
- 658 Follows, M., R. G. Williams, and J. C. Marshall (1996), The solubility pump of carbon in
659 the subtropical gyre of the North Atlantic, *Journal of Marine Research*, 54, 605–630.
- 660 Follows, M. J., T. Ito, and J. Marotzke (2002), The wind-driven, subtropical gyres
661 and the solubility pump of CO₂, *Global Biogeochemical Cycles*, 16(4), doi:10.1029/
662 2001GB001786.
- 663 Gebbie, G., and P. Huybers (2006), Meridional circulation during the Last Glacial Max-
664 imum explored through a combination of South Atlantic $\delta^{18}\text{O}$ observations and a
665 geostrophic inverse model, *Geochemistry, Geophysics, Geosystems*, 7(11), doi:10.1029/
666 2006GC001383.
- 667 Gnanadesikan, A. (1999), A Simple Predictive Model for the Structure of the Oceanic
668 Pycnocline, *Science*, 283, 2077–2079.
- 669 Goodwin, P., R. G. Williams, M. J. Follows, and S. Dutkiewicz (2007), Ocean-atmosphere
670 partitioning of anthropogenic carbon dioxide on centennial timescales, *Global Biogeo-*
671 *chemical Cycles*, 21, doi:10.1029/2006GB002810.

- 672 Goodwin, P., M. J. Follows, and R. G. Williams (2008), Analytical relationships between
673 atmospheric carbon dioxide, carbon emissions, and ocean processes, *Global Biogeochem-*
674 *ical Cycles*, *22*, GB3030, doi:10.1029/2008GB003184.
- 675 Goodwin, P., R. G. Williams, A. Ridgwell, and M. J. Follows (2009), Climate sensitivity
676 to the carbon cycle modulated by past and future changes in ocean chemistry, *Nature*
677 *Geoscience*, *2*, 145–150, doi:10.1028/NGE0416.
- 678 Huybers, P., G. Gebbie, and O. Marchal (2007), Can Paleoceanographic Tracers
679 Constrain Meridional Circulation Rates?, *Journal of Physical Oceanography*, *37*,
680 doi:10.1175/JPO3018.1.
- 681 Ito, T., and M. J. Follows (2003), Upper ocean control on the solubility pump of CO₂,
682 *Journal of Marine Research*, *61*, 465–489.
- 683 Knox, F., and M. McElroy (1984), Changes in atmospheric CO₂: Influence of biota at
684 high latitudes, *Journal of Geophysical Research*, *89*, 4629–4637.
- 685 Kwon, E.-Y., and F. Primeau (2006), Optimization and sensitivity study of a biogeochem-
686 istry ocean model using an implicit solver and in-situ phosphate data, *Global Biogeo-*
687 *chemical Cycles*, *20*, doi:10.1029/2005GB002631.
- 688 Kwon, E.-Y., and F. Primeau (2008), Optimization and sensitivity study of a global bio-
689 geochemistry ocean model using combined in-situ DIC, alkalinity and phosphate data,
690 *Journal of Geophysical Research - Oceans*, *113*(C08011), doi:10.1029/2007JC004520.
- 691 Ledwell, J. R., A. J. Watson, and C. S. Law (1993), Evidence for slow mixing across the
692 pycnocline from an open-ocean tracer release experiment, *Nature*, *364*, 701–703.
- 693 LeGrand, P., and K. Alverson (2001), Variations in atmospheric CO₂ during glacial cycles
694 from an inverse modeling perspective, *Paleoceanography*, *16*, 604–616.

- 695 Locarnini, R. A., A. V. Mishonov, J. I. Antonov, T. P. Boyer, , and H. E. Garcia (2006),
696 Volume 1: Temperature, in *NOAA Atlas NESDIS*, vol. 62, edited by S. Levitus, U.S.
697 Government Printing Office, Washington, D.C.
- 698 Lüthi, D., et al. (2008), High-resolution carbon dioxide concentration record 650,000-
699 800,000 years before present, *Nature*, *453*, 379–382.
- 700 Marinov, I., A. Gnanadesikan, J. R. Toggweiler, and J. L. Sarmiento (2006), The Southern
701 Ocean Biogeochemical Divide, *Nature*, *441*, 964–967.
- 702 Marinov, I., M. Follows, A. Gnanadesikan, J. L. Sarmiento, and R. D. Slater (2008a),
703 How does ocean biology affect atmospheric pCO₂? Theory and models, *Journal of*
704 *Geophysical Research*, *113*, doi:10.1029/2007JC004598.
- 705 Marinov, I., A. Gnanadesikan, J. L. Sarmiento, J. R. Toggweiler, M. Follows, and B. K.
706 Mignone (2008b), Impact of ocean circulation on biological carbon storage in the ocean
707 and atmospheric pCO₂, *Global Biogeochemical Cycles*, *22*, doi:10.1029/2007GB002958.
- 708 Paul, A., and C. Schafer-Neth (2003), Modeling the water masses of the Atlantic Ocean
709 at the Last Glacial Maximum, *Paleoceanography*, *18*(3), doi:10.1029/2002PA000783.
- 710 Petit, J., et al. (1999), Climate and atmospheric history of the past 420,000 years from
711 the Vostok ice core, Antarctica, *Nature*, *399*, 429–436.
- 712 Primeau, F. W. (2005), Characterizing transport between the surface mixed layer and
713 the ocean interior with a forward and adjoint global ocean transport model, *Journal of*
714 *Physical Oceanography*, *35*(2), 545–564.
- 715 Primeau, F. W., and M. Holzer (2006), The Ocean’s Memory of the Atmosphere:
716 Residence-Time and Ventilation-Rate Distributions of Water Masses, *Journal of Phys-*
717 *ical Oceanography*, *36*, 1439–1456.

- 718 Sarmiento, J. L., and R. J. Toggweiler (1984), A new model for the role of the oceans in
719 determining atmospheric pCO₂, *Nature*, *308*, 621–624.
- 720 Siegenthaler, U., and T. Wenk (1984), Rapid atmospheric CO₂ variations and ocean
721 circulation, *Nature*, *308*, 624–625.
- 722 Siegenthaler, U., et al. (2005), Stable Carbon Cycle-Climate Relationship During the Late
723 Pleistocene, *Science*, *310*(5752), 1313–1317.
- 724 Sigman, D. M., and E. A. Boyle (2000), Glacial/interglacial variations in atmospheric
725 carbon dioxide, *Nature*, *407*, 859–869.
- 726 Toggweiler, J., A. Gnanadesikan, S. Carson, R. Murnane, and J. Sarmiento (2003), Rep-
727 resentation of the carbon cycle in box models and GCMs: 1. Solubility pump, *Global*
728 *Biogeochemical Cycles*, *17*(1), 1026.
- 729 Volk, T., and M. I. Hoffert (1985), Ocean carbon pumps: Analysis of relative strengths
730 and efficiencies in ocean-driven atmospheric CO₂ changes, in *The Carbon Cycle and*
731 *Atmospheric CO₂: Natural Variations Archaen to Present*, *Geophysical Monograph Se-*
732 *ries*, vol. 32, edited by E. Sundquist and W. Broecker, pp. 99–110, AGU, Washington,
733 D.C.
- 734 Wunsch, C. (2003), Determining paleoceanographic circulations, with emphasis on the
735 Last Glacial Maximum, *Quaternary Science Reviews*, *22*, 371–385.
- 736 Zeebe, R. E., and D. Wolf-Gladrow (2001), *CO₂ in Seawater: Equilibrium, Kinetics,*
737 *Isotopes*, 346 pp., Elsevier Oceanography Series, Amsterdam.

Figure 1. Schematic diagram showing the net flow of carbon between the atmosphere, surface ocean and deep ocean associated with a cooling of the low-latitude surface ocean. The diagram shows the Atlantic ocean basin since this is where most of the ocean's deep waters form. The general sense of large-scale ocean circulation is redrawn from *Marinov et al.* [2006]. The upper (red) circulation is dominated by a clockwise rotating cell in which low-latitude water flows northward at the surface and is returned southward at depth as North Atlantic Deep Water (NADW). The upper circulation sits on top of the deep (blue) circulation – a counter-clockwise rotating cell with northward-flowing Antarctic Bottom Water (AABW) at depth. Antarctic Intermediate Water (AAIW) forms part of the upper ocean circulation as it is entrained into the thermocline. An eddy return flow transports low-latitude waters into the Southern Ocean [*Gnanadesikan, 1999*]. Subduction of mode waters ventilates the thermoclines of the subtropical gyres. In response to the cooling perturbation, CO_2 invades the ocean in the low-latitudes. DIC is subducted downward into the thermocline (blue shading), and mixes into the interior ocean. Transport of DIC-enriched surface waters poleward causes anomalous outgassing in the high latitudes. This outgassing represents a negative feedback that tends to damp the atmospheric $p\text{CO}_2$ decrease. How much the atmospheric $p\text{CO}_2$ drops in response to the cooling (i.e. the low-latitude sensitivity) depends on how much of the ocean is ventilated directly from the low latitudes, and on how well the high-latitude surface waters equilibrate with the atmosphere. Low-latitude sensitivity is enhanced by both an increase in the volume of low-latitude waters, and by inhibited gas exchange in high-latitude regions.

Figure 2. Plot of the Green function $\mathcal{G}(\mathbf{r}_s)$ for OGCM run S1. Note the logarithmic scale. Ω_L is defined on the ocean surface between 45°N and 45°S. Ω_H is defined on the ocean surface outside Ω_L . The plot shows mode waters forming in some areas of the low latitudes, while the major ventilation sites (red) lie in the North Atlantic and Southern Ocean regions. The units of meters result from dividing the volume of the ocean ventilated at each grid point \mathbf{r}_s by the surface area of each grid point.

Figure 3. Box model configurations. (a) The 3-box model consists of 3 ocean boxes H, L, and D, representing the high-latitude, low-latitude, and deep oceans respectively, coupled to an atmospheric box A. The overturning circulation T is set to 20 Sv and the high-latitude mixing term f_{hd} to 60 Sv. The gas exchange coefficient k_{ge} for the H and L boxes is proportional to the CO₂ solubility and surface area with a piston velocity of 5.5×10^{-5} m/s. Box H has a depth of 250 m and covers 15% of the sea surface, while box L has a depth of 100 m and covers 85% of the sea surface. (b) The 5 box model is modified from the 3 box model to include both tropical (T) and subtropical (S) surface ocean boxes. The cold (blue) overturning T_c is set to 20 Sv, while the warm (red) overturning T_w , which ventilates the thermocline, is set to 5 Sv. The thickness of box H is 1000 m, and the thickness of the thermocline box (M) is 900 m. Box T has a temperature of 25 °C and box S has a temperature of 17°C. Boxes S and T each cover 42.5% of the ocean surface area. All other model parameters are the same as in the 3 box model.

Figure 4. (a) The magnitude of the low-latitude ventilation effect scales linearly with the amount of water ventilated from low latitudes, expressed in this plot as the fraction of the total ocean volume ventilated from low latitudes. Higher low-latitude sensitivities are associated with larger volumes of low-latitude water. The scatter in the plot is due to the fact that the inertia M_{oa} , which depends on the buffering capacity of the ocean, is not constant across all model runs – accounting for this effect eliminates the scatter (inset plot). (b) The magnitude of the air-sea disequilibrium effect in the northern high latitudes scales linearly with the product of the strength of the Atlantic meridional overturning circulation (AMOC) and the fraction of the ocean ventilated from the northern high latitudes, in agreement with the relationship derived in Section 4.2 and the Appendix. The magnitude of the disequilibrium effect in the Southern Ocean is generally smaller and less variable in our OGCM runs than that in the northern high latitudes (inset plot).

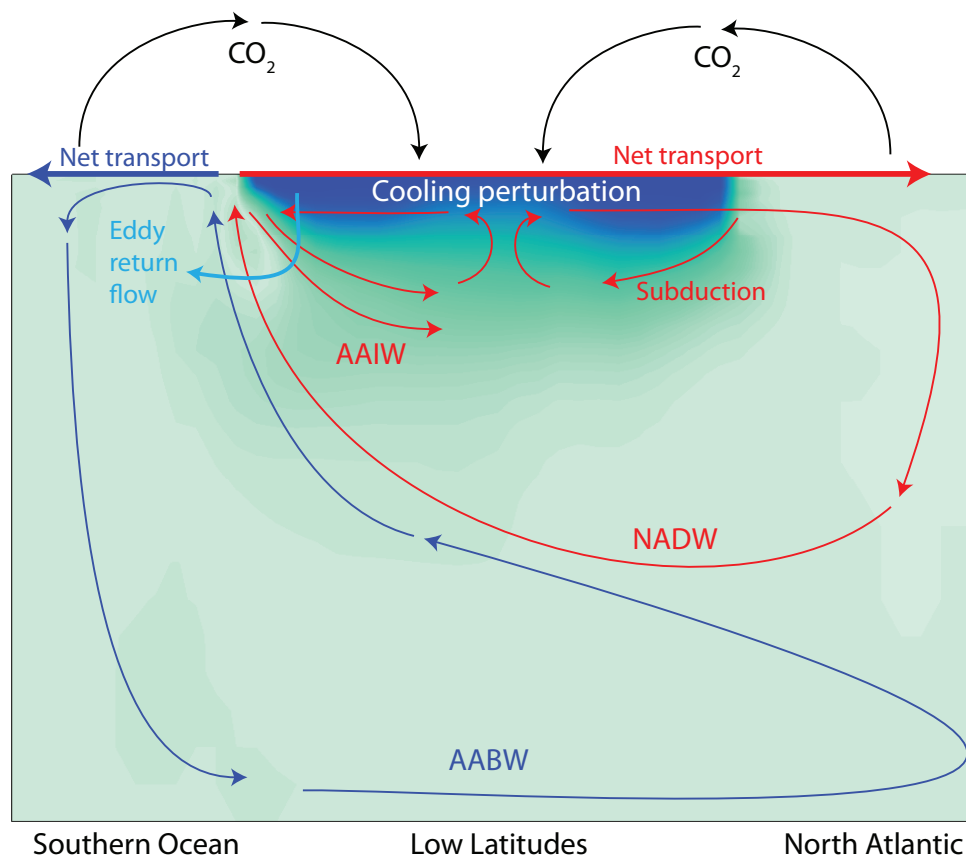


Figure 1.

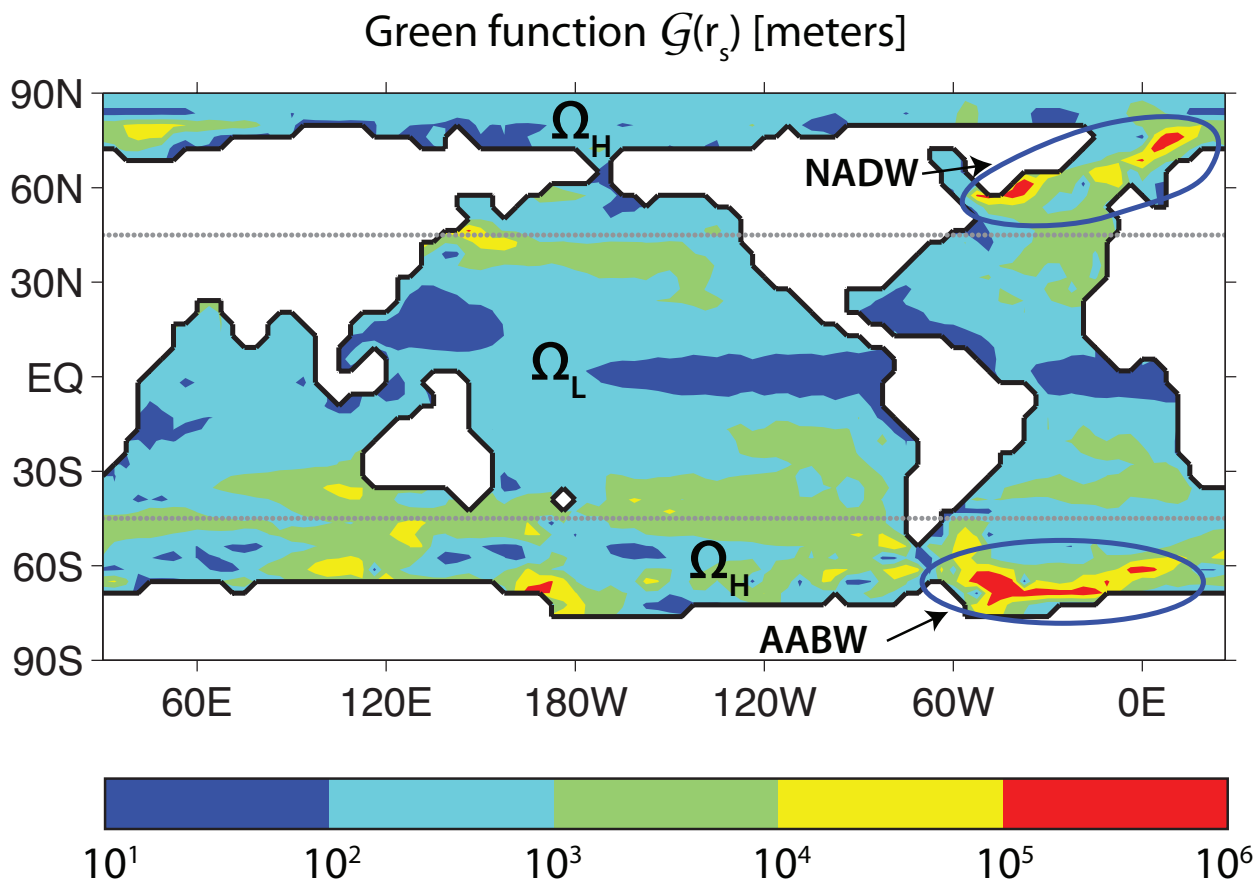
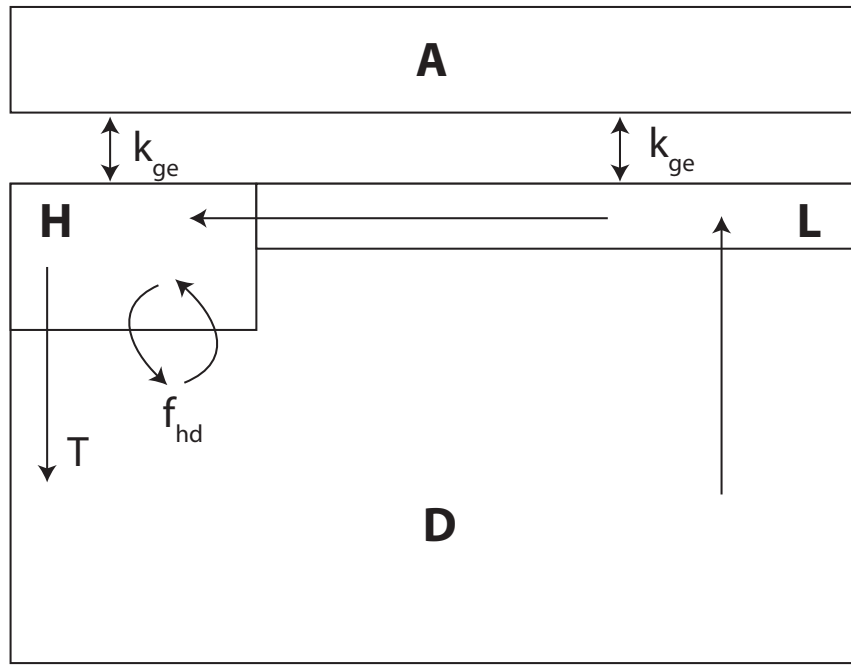
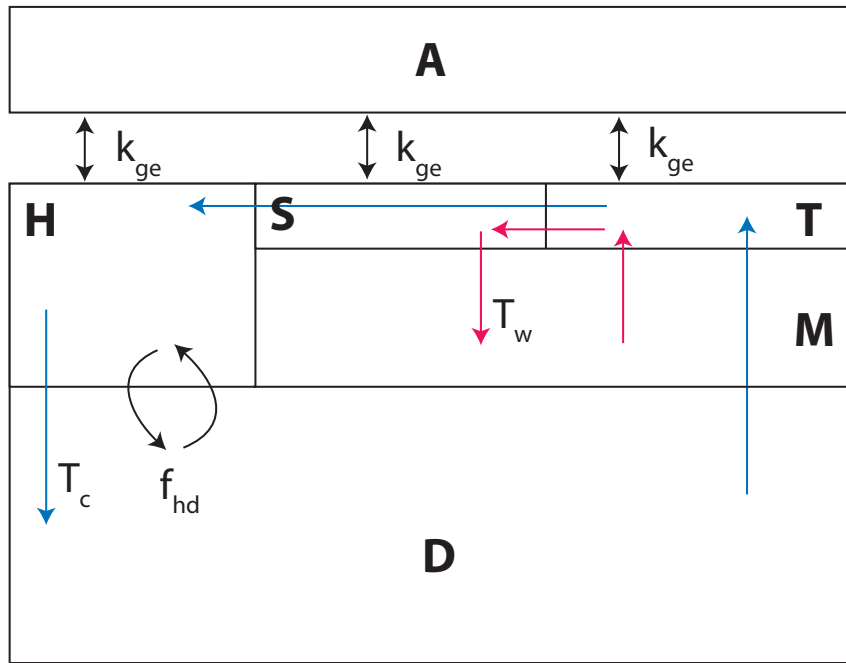


Figure 2.



(a) 3-box model



(b) 5-box model

Figure 3.

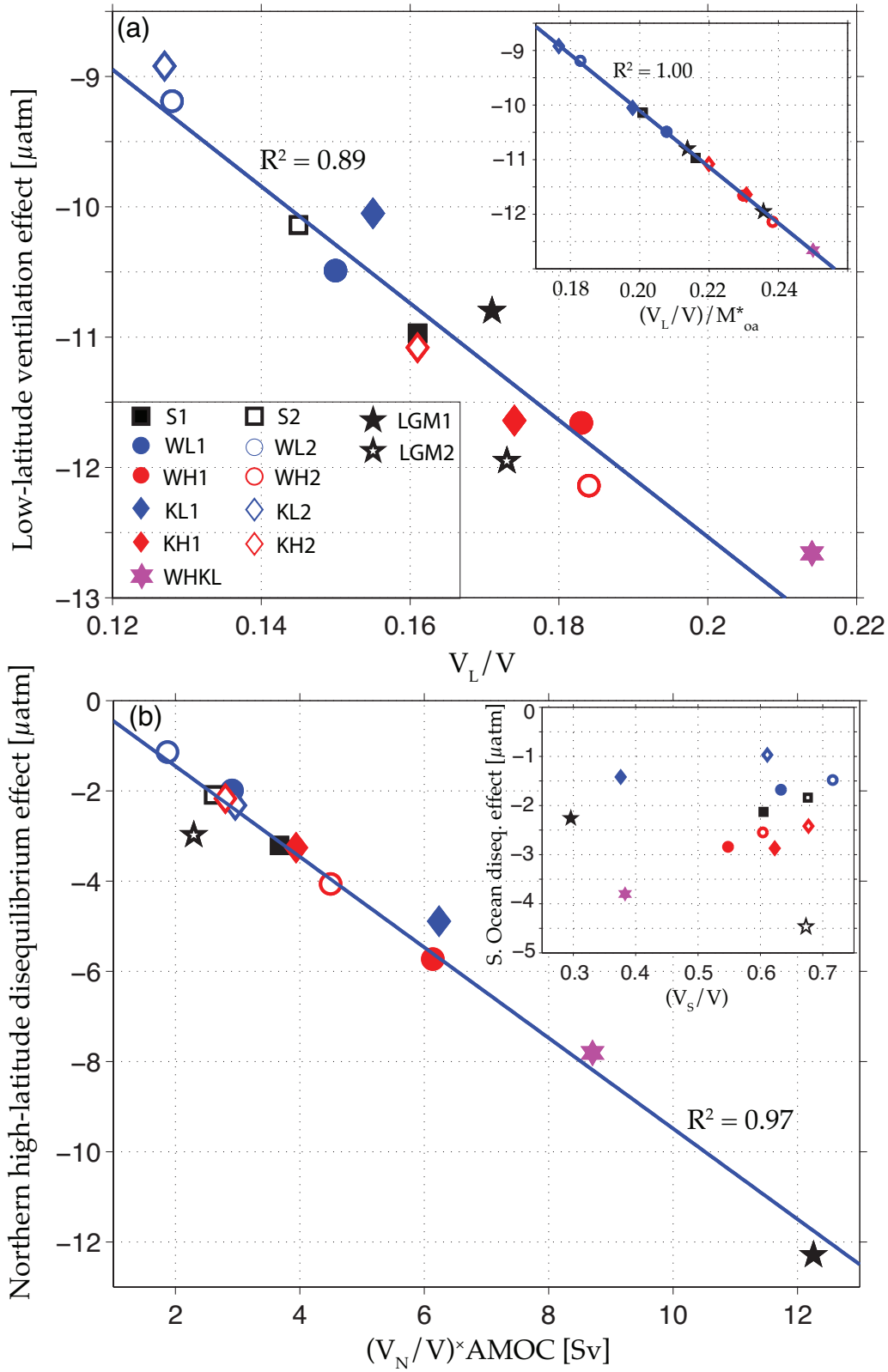


Figure 4.

Table 1. Boundary conditions and parameters used to obtain new circulations in the OGCM. The “Modern” runs simulate a range of circulations using modern temperature and salinity forcing. The control (C) temperature and salinity is the climatology used in *Primeau* [2005], while WOA05 indicates the World Ocean Atlas 2005 objectively-analyzed monthly mean sea-surface temperature [*Locarnini et al.*, 2006] and salinity [*Antonov et al.*, 2006] averaged over the top 50 m of the ocean. Perturbations from each of the basic states are obtained by increasing or decreasing the zonal wind stress or the background vertical diffusivity. “LGM” runs present two possible glacial circulation states obtained using the GLAMAP last glacial maximum temperature and salinity reconstructions described in *Paul and Schafer-Neth* [2003]. We used the “core” version of the data set available on-line at ftp://ftp.ncdc.noaa.gov/pub/data/paleo/paleocean/by_contributor/paul2003. PSN+1 adds a 1 psu salinity anomaly in the Weddell Sea as suggested by *Paul and Schafer-Neth* [2003], while PSN omits this anomaly. The units of K_v are cm^2/s .

“Modern” Runs								
Run	Temperature and Salinity		Wind stress			Vertical diffusivity K_v		
	C	WOA05	C	Cx0.5	Cx2	0.5	0.15	0.85
S1	•		•			•		
WL1	•			•		•		
WH1	•				•	•		
KL1	•		•				•	
KH1	•		•					•
WHKL	•				•	•		
S2		•	•			•		
WL2		•		•		•		
WH2		•			•	•		
KL2		•	•				•	
KH2		•	•					•
“LGM” Runs								
Run	Temperature and Salinity		Wind stress			Vertical diffusivity K_v		
	PSN	PSN+1	C	Cx0.5	Cx2	0.5	0.15	0.85
LGM1	•		•			•		
LGM2		•	•			•		

Table 2. Change in atmospheric $p\text{CO}_2$ for the box models and OGCM due to a temperature decrease of 6 °C in the low-latitude patch. Also shown are changes in $p\text{CO}_2^{atm}$ partitioned according to the change due to the low-latitude ventilation effect, and the high- and low-latitude disequilibrium effects. The quantities in the last three columns correspond to the three terms on the right hand side of Eq. (8), divided by the inertia M_{oa} . Values in parentheses are results from the fast gas exchange runs. Units are μatm .

Model	Perturbed patch	$\delta p\text{CO}_2^{atm}$	Low-latitude ventilation effect	High-latitude disequilibrium effect	Low-latitude disequilibrium effect
3 Box	Box L	-6.42 (-1.73)	-1.62 (-1.68)	-4.86 (-0.06)	0.06 (0.00)
5 Box	Box S and T	-9.37 (-4.72)	-4.58 (-4.67)	-4.83 (-0.05)	0.04 (0.00)
OGCM	45°S - 45°N	-15.70 (-11.25)	-10.97 (-11.24)	-5.34 (-0.01)	0.60 (0.00)

Table 3. As in Table 2 except for the OGCM sensitivity runs. Run S1 is the OGCM analyzed in Table 2. Only results from models with normal gas exchange are shown. All units are μatm .

Run	$\delta p\text{CO}_2^{atm}$	Low-latitude ventilation effect	High-latitude disequilibrium effect	Low-latitude disequilibrium effect
S1	-15.70	-10.97	-5.34	0.60
WL1	-13.56	-10.49	-3.67	0.61
WH1	-19.55	-11.66	-8.57	0.68
KL1	-15.88	-10.05	-6.31	0.48
KH1	-17.05	-11.64	-6.13	0.73
WHKL	-23.37	-12.66	-11.61	0.90
S2	-13.44	-10.14	-3.93	0.64
WL2	-11.30	-9.19	-2.62	0.51
WH2	-17.67	-12.14	-6.61	1.08
KL2	-11.48	-8.92	-3.29	0.72
KH2	-14.90	-11.08	-4.59	0.77
LGM1	-24.66	-10.80	-14.55	0.69
LGM2	-18.73	-11.95	-7.44	0.66

Table 4. Quantities that are relevant to the low-latitude sensitivity for the OGCM runs. V_L is the volume of the ocean ventilated from low latitudes ($45^\circ\text{S} - 45^\circ\text{N}$), and V_N is the volume of the ocean ventilated from the northern high latitudes (north of 45°N). V is the total ocean volume. AMOC is the maximum strength of the Atlantic meridional overturning circulation north of 45°S . M_{oa}^* is a reduced inertia defined $M_{oa}^* \equiv M_{oa}/(M_a + f_0 \int \mathcal{G} d^2 r_s)$, where $f_0 = 1024.5$ mol/m³.

Run	$\delta p\text{CO}_2^{atm}$ (μatm)	V_L/V (unitless)	V_N/V (unitless)	AMOC (Sv)	M_{oa}^* (unitless)
S1	-15.70	0.161	0.234	15.7	0.745
WL1	-13.56	0.150	0.217	13.4	0.722
WH1	-19.55	0.183	0.269	22.8	0.796
KL1	-15.88	0.155	0.469	13.3	0.783
KH1	-17.05	0.174	0.203	19.4	0.754
WHKL	-23.37	0.214	0.403	21.6	0.856
S2	-13.44	0.145	0.179	14.6	0.722
WL2	-11.30	0.128	0.156	12.0	0.700
WH2	-17.67	0.184	0.212	21.2	0.772
KL2	-11.48	0.127	0.262	11.3	0.719
KH2	-14.90	0.161	0.162	17.3	0.732
LGM1	-24.66	0.171	0.533	23.0	0.800
LGM2	-18.73	0.173	0.154	14.9	0.734